

Bioimpedance modeling to monitor astrocytic response to chronically implanted electrodes

This article has been downloaded from IOPscience. Please scroll down to see the full text article.

2009 J. Neural Eng. 6 055005

(<http://iopscience.iop.org/1741-2552/6/5/055005>)

[The Table of Contents](#) and [more related content](#) is available

Download details:

IP Address: 130.207.50.192

The article was downloaded on 02/04/2010 at 14:53

Please note that [terms and conditions apply](#).

Bioimpedance modeling to monitor astrocytic response to chronically implanted electrodes

G C McConnell¹, R J Butera^{1,2} and R V Bellamkonda¹

¹ Wallace H Coulter Department of Biomedical Engineering, Georgia Institute of Technology/Emory University, 313 Ferst Drive, Atlanta, GA 30332, USA

² School of Electrical and Computer Engineering, Georgia Institute of Technology, Atlanta, GA, USA

E-mail: rbutera@ece.gatech.edu and ravi@gatech.edu

Received 16 October 2008

Accepted for publication 10 March 2009

Published 1 September 2009

Online at stacks.iop.org/JNE/6/055005

Abstract

The widespread adoption of neural prosthetic devices is currently hindered by our inability to reliably record neural signals from chronically implanted electrodes. The extent to which the local tissue response to implanted electrodes influences recording failure is not well understood. To investigate this phenomenon, impedance spectroscopy has shown promise for use as a non-invasive tool to estimate the local tissue response to microelectrodes. Here, we model impedance spectra from chronically implanted rats using the well-established Cole model, and perform a correlation analysis of modeled parameters with histological markers of astroglial scar, including glial fibrillary acid protein (GFAP) and 4',6-diamidino-2-phenylindole (DAPI). Correlations between modeled parameters and GFAP were significant for three parameters studied: P_y value, R_o and $|Z|_{1\text{ kHz}}$, and in all cases were confined to the first 100 μm from the interface. P_y value was the only parameter also correlated with DAPI in the first 100 μm . Our experimental results, along with computer simulations, suggest that astrocytes are a predominant cellular player affecting electrical impedance spectra. The results also suggest that the largest contribution from reactive astrocytes on impedance spectra occurs in the first 100 μm from the interface, where electrodes are most likely to record electrical signals. These results form the basis for future approaches where impedance spectroscopy can be used to evaluate neural implants, evaluate strategies to minimize scar and potentially develop closed-loop prosthetic devices.

(Some figures in this article are in colour only in the electronic version)

1. Introduction

Neural prosthetics is a burgeoning field with clinical applications in the treatment of spinal cord injuries, amyotrophic lateral sclerosis (ALS) and other debilitating diseases/injuries [1, 2]. However, the widespread usefulness of neural prosthetics is currently hindered by the inability to reliably record neural signals for durations beyond several months. To assess the contribution of local tissue response to chronic recording failure, there is an urgent need to develop tools to non-invasively determine the extent of local tissue response surrounding microelectrodes.

The time course of the tissue response to microelectrodes is well defined, and culminates in the formation of a glial scar, composed primarily of reactive astrocytes [3–7]. The gold standard for determining the degree of tissue reaction surrounding microelectrodes is histology. Gross histological stains, such as hematoxylin and eosin, have been complemented by the advancement of immunohistochemical methods to allow the visualization of specific proteins. The disadvantages of these methods are (1) an inability to follow the tissue reaction time course in a living animal, (2) the large amount of time and labor required for histological work and (3) the qualitative nature of assessment. Establishing a

quantitative, non-destructive method to assess the degree of tissue reaction surrounding microelectrodes would expedite study of the influence of tissue reaction on the reliability of microelectrode recordings. Furthermore, such a technique would be invaluable for evaluating the efficacy of novel strategies to improve chronic recording reliability.

While the magnitude of the impedance at 1 kHz is a common measure for assessing the performance of chronic electrodes, measuring impedance at multiple frequencies has several advantages due to the ability to then model the impedance spectra. The advantages of multiple frequencies over one frequency have been an area of contention in the field of body impedance analysis (BIA); however, modeling of multiple frequencies using the Cole model results in more accurate predictions [8, 9].

The biophysics of the passive electrical properties of heterogeneous material, including biological tissue, has been intensely studied for over 60 years [10, 11]. The complex permittivity of biological tissue is known to vary as a function of frequency [9, 12]. In the 1 kHz to 10 MHz frequency range, the electric field penetrates across cellular membranes in biological tissue. This frequency range, called the β dispersion, is useful in predicting changes in the structure of biological tissue [13].

Pioneering work by Williams *et al* showed that impedance spectra in the β dispersion from chronic microelectrodes display a characteristic feature for tissue reaction when plotted in the complex plane [14]. Implants surrounded by severe tissue reactions, as assessed using 4',6-diamidino-2-phenylindole (DAPI) and glial fibrillary acid protein (GFAP), showed a more pronounced circular arc in the complex plane. This circular arc locus in the complex plane is not, however, unique to chronic microelectrodes in the brain. Indeed, it occurs in impedance measurements of all biological tissues [13]. The characteristic semicircle with the center depressed below the real axis is empirically expressed in the Cole equation [10]:

$$Z = R_{\infty} + \frac{\Delta R}{1 + (j\omega\tau_c)^{\alpha}}, \quad (1)$$

where $\Delta R = R_0 - R_{\infty}$ and $\tau_c = 1/\omega_c = 1/(2\pi f_c)$. In (1), Z is complex impedance at frequency ω and $j = \sqrt{-1}$. The impedance circular arc locus is fully defined by four independent variables: R_0 : resistance at zero frequency, R_{∞} : resistance at infinite frequency, α : the angle of depression ranging between 0 and 1 and f_c : the characteristic frequency, which defines the frequency scale. Because of the advantages of bioimpedance modeling over measurement of a single frequency such as 1 kHz, along with the wide use of the Cole model to relate impedance spectroscopy to tissue structure [9, 13, 15–19], we chose to study the usefulness of Cole model parameters for estimating the tissue response to chronic microelectrode arrays. An index derived from the Cole model parameters R_0 and R_{∞} , the Py value, was also investigated. The Py value, $\Delta R/R_0$, represents the normalized extent of the β dispersion and has been shown to be highly correlated with cell volume fraction in cell suspensions [20]. Cell volume fraction is the ratio of intracellular volume to total tissue volume (both intracellular and extracellular volumes

combined). Since astrocyte proliferation and hypertrophy are known to occur in the glial scar, both of which affect cell volume fraction, we hypothesized that Py might be correlated with these changes.

In this study, we present our work on the application of bioimpedance modeling for the estimation of the tissue response to chronic microelectrodes. Correlation results of modeling parameters with histology show that three parameters, Py , R_0 and $|Z|_{1\text{ kHz}}$, are significantly correlated with reactive astrocytes in the first 100 μm surrounding microelectrodes.

2. Materials and methods

2.1. Surgical procedures for chronic implants

Four adult male Sprague-Dawley rats (275–299 g) were implanted with 304 grade stainless steel microwires, 200 μm in diameter and 300–500 k Ω impedance at 1 kHz, insulated with epoxy (part number UESSFESEBNNC; FHC, Inc.). All implanted materials were sterilized using ethylene oxide at least 48 h prior to surgeries. Rats were anesthetized for 5 min with a mixture of 5% isoflurane and 1 L min^{-1} prior to surgery. Each rat was positioned in a stereotactic frame (Kopf), where anesthesia was maintained to effect (1–3% isoflurane and 0.3 L min^{-1}) during surgery by monitoring the rat's breathing. The rat's head was shaven over the incision area and the skin was disinfected with isopropyl alcohol and chlorohexadorm using a slight scrubbing motion prior to making the incision. Ophthalmic ointment was applied to the eyes to prevent drying. A midline incision was made along the scalp, the skin retracted, and the periosteum cleared to expose the bregma. Five stainless steel skull screws were inserted (dimensions = 0–80 \times (1/16); Plastics One, Inc.). One skull screw (0 mm lateral and \sim 2 mm posterior to the Lambda) was wrapped with fine metal wire soldered to a Molex connector to serve as the counter electrode (CE) during impedance measurements. A dental drill was used to create a 3.2 mm hole at 0.2 mm anterior and 3.0 mm lateral to the bregma with a custom trephine (24 tooth \times 3 mm O.D.) fabricated from stainless steel tubing (Small Parts). In order to minimize iatrogenic damage, room-temperature saline was applied liberally to the spinning drill bit at the bone interface. The bone plug was carefully removed and, with the aid of a surgical scope, the dura was gently pierced using a 28 gauge needle with the tip bent at a 45° angle, cut using dura scissors and then reflected back over the skull. Two electrodes were implanted, one in each hemisphere, of the motor cortex region (\pm 3 mm lateral and 0.2 mm anterior to the bregma). The microwires were implanted \sim 1 mm below the surface of the cortex using a stereotaxic apparatus at a rate of \sim 0.1 mm s^{-1} . After 5 min, during which the brain surface was kept moist with saline, the craniotomy was covered with 1% SeaKem Agarose (Cambrex) gel in phosphate buffered saline (PBS). The craniotomies were further sealed and protected using dental acrylic, which was anchored to the skull by the bone screws. All implants were performed by the

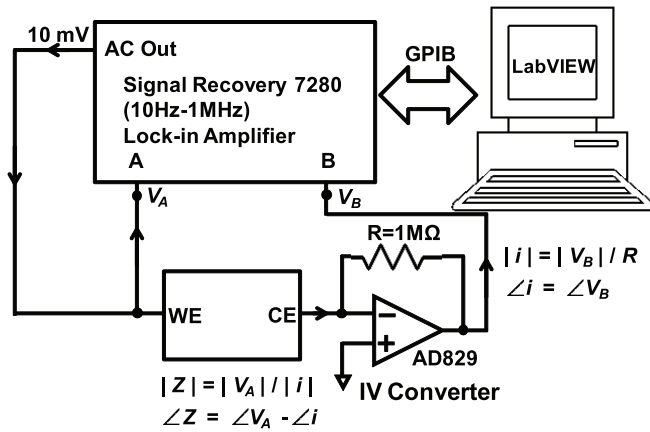


Figure 1. Schematic showing the setup used to measure electrical impedance spectra. The setup consists of a lock-in amplifier with a constant voltage output of 10 mV connected to the working electrode (WE) and measured at input A. The counter electrode (CE) is connected to an current-to-voltage converter and the voltage measured at input B. Physically, WE: microwire and CE: skull screw.

same surgeon. All procedures were approved by Georgia Tech Institutional Animal Care and Use Committee.

2.2. Impedance analysis: impedance spectroscopy measurement

The cellular characteristics of the glial scar change little from 6 weeks to 12 weeks [5]. After 11 weeks, a time point long after the electrical properties of the astroglial scar have stabilized, the electrical impedance spectra of the electrode–tissue interface were measured. A constant voltage AC 10 mV signal was applied to the microelectrode, and impedance magnitude and phase were measured at a counter electrode (stainless steel skull screw), located at a fixed distance away, from 100 Hz to 1 MHz using a logarithmic sweep of 40 points, and additionally at 1 kHz. No DC bias voltage was applied to the electrode. Impedance sweeps were measured twice for each microelectrode and the average was used in further analysis. Constant voltage, as opposed to constant current, was used to minimize the contribution of parasitic impedance, in parallel with the electrode–tissue impedance. The measurement setup consisted of a lock-in amplifier (Signal Recovery Model 7280) along with a current-to-voltage converter (figure 1). For the current-to-voltage converter, a high-speed op-amp, AD829 (Analog Devices), was chosen for its high gain bandwidth product (GBWP) of 120 MHz. Impedance magnitude and phase were calculated using the voltage measured at input A and at input B. Both inputs could not be read simultaneously, so two sweeps were made sequentially: one for input A and one for input B. The tissue properties were assumed to be stable over the course of the measurement, which is reasonable given that each sweep took ~30 s to complete, and sweeps were made consecutively. Additional impedance sweeps were made after the removal of the electrode in PBS in order to test the electrical properties of the electrode alone.

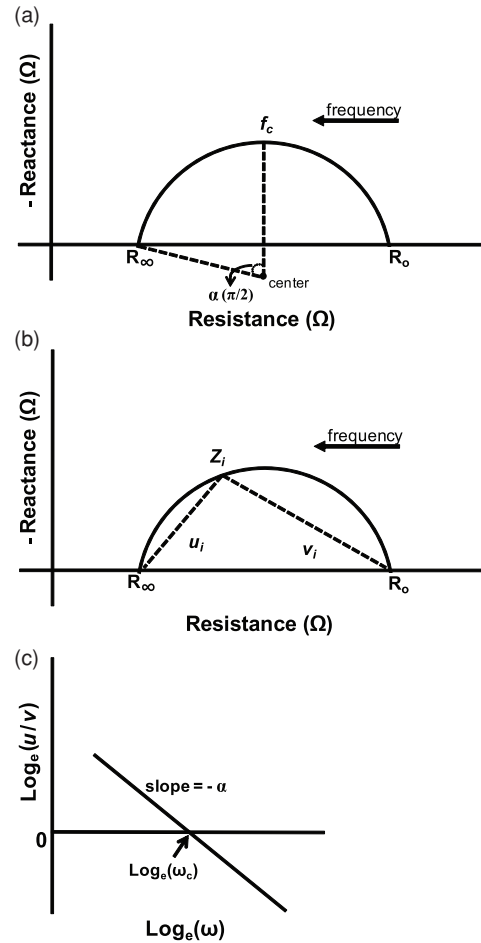


Figure 2. (a) Theoretical impedance spectra of biological tissue showing the Cole model parameters. The four Cole model parameters can be estimated geometrically from the impedance loci plot to characterize the impedance spectra. R_0 and R_∞ are the resistances at zero and infinite frequency, respectively; f_c , characteristic frequency, is the frequency at which the reactive component of impedance is maximal; α is the angle of depression of the center of the circle below the real axis. (b)–(c) Calculation of the Cole model parameters f_c and α . (b) The chord lengths, u_i and v_i , are calculated at each complex impedance value, Z_i . (c) Theoretical plot showing the relationship between chord lengths and the Cole parameters f_c , where $f_c = 2\pi/\omega_c$, and α .

2.3. Impedance analysis: estimation of Cole parameters and P_y from impedance spectra

Data points from the complex impedance locus plot, with the real part of the impedance versus the negative imaginary part of the impedance, were selected to optimally fit to a circle using least-squares minimization [21]. The best-fit curves all had a goodness of fit of $r > 0.99$ and impedance from a minimum of ten frequencies was modeled. The zero intercepts of the curves were then calculated (R_0 and R_∞). From these two parameters, P_y was calculated using the formula $(R_0 - R_\infty)/R_0$ (see figure 2(a)). The characteristic frequency, f_c , and parameter α were calculated using the ‘ln(u/v)’ method [12, 22] (see figures 2(b) and (c)). Briefly, the chord lengths u_i and v_i are calculated for all complex impedance values, Z_i (figure 2(b)). f_c and α can then be determined

from the plot of $\log(u/v)$ versus $\log(f)$ by the x -intercept and the negative slope, respectively (figure 2(c)).

2.4. Tissue analysis: brain tissue preparation for immunohistochemistry

Rats were perfused transcardially with 200 mL of PBS, followed by 200 mL of 4% paraformaldehyde in PBS \sim 12 h after impedance spectroscopy measurement. We assumed that changes in the tissue between when the impedance was measured and when the animal was sacrificed were minor, since relatively little variability in electrode impedance occurs after 4 weeks [23]. The acrylic headcap, attached to the skull, along with the electrodes were carefully removed and stored in PBS at 4 °C. The brain was then extracted and left in 4% paraformaldehyde solution overnight at 4 °C. Brains were then transferred to PBS for 1 h at 4 °C, followed by 30% sucrose until they had sunk to the bottom (\sim 2–3 days). Brains were then cryoembedded using optimal cutting temperature (OCT) compound, cryosectioned to a thickness of 30 μ m, and stored sequentially to preserve cortical depth information.

2.5. Tissue analysis: immunohistochemistry

Cell density and cell hypertrophy strongly influence the electrical impedance properties of tissue within the β dispersion frequency band, due to their relationship with cell volume fraction [24]. Therefore, GFAP expression, which is upregulated in response to injury, was used to estimate astrocyte hypertrophy. DAPI, which stains all cell nuclei, was used to estimate cell density.

Four tissue sections from each brain at cortical depths of \sim 200 μ m, \sim 500 μ m, \sim 800 μ m and \sim 1100 μ m were processed. Tissue sections were incubated in blocking solution, consisting of 4% goat serum in PBS, for 1 h at room temperature. Sections were then incubated in primary antibody solution, GFAP (DAKO, 1:2000) in blocking solution, overnight at 4 °C. Following three rinses in PBS, sections were incubated in secondary antibody solution, Alexa 488 IgG anti-rabbit (Molecular Probes, 1:220), for 1 h at room temperature. After three rinses, sections were counterstained with DAPI (Invitrogen), mounted onto slides and coverslipped using Fluoromount G.

2.6. Tissue analysis: quantitative analysis of histological images

Fluorescent images were acquired using a Microfire digital camera attached to a Zeiss Axioscop2 Plus upright microscope with a 10 \times objective. A minimum of three tissue sections approximately 200 μ m, 500 μ m and 800 μ m below the brain surface were imaged for further quantification. All tissue sections were imaged in a single session to minimize variability. The exposure time was consistent within each marker and was set below saturation of the digital camera. Fluorescent intensity as a function of distance from the electrode–tissue interface was calculated using a custom program written in MATLAB (Mathworks) [25]. Briefly, the recording track was outlined using GFAP-labeled images, and

an ellipse was computed from five or more user-specified points to delineate the border between the electrode track and the surrounding tissue. Rectangular regions were drawn 500 μ m away from the border on both the left and right sides of the electrode track, with the width of the quantified region approximately equal to the diameter of the electrode track. The intensity values of each of the boxed regions were then averaged along the y -axis. For normalization, the average intensity from 400 to 500 μ m in each image was subtracted from the intensity profile 0–500 μ m. The integral of the mean intensity profile at four different distance increments along the electrode (0–100 μ m, 100–200 μ m, 200–300 μ m and 300–500 μ m) was also calculated for each image.

2.7. Computer modeling

Computer simulations were constructed using software previously developed for the study of the relationship between tissue structure and its passive electrical impedance properties (Bioimpedance Simulator; source files are available at <http://www.cnm.es/~mtrans/BioZsim/>) [26]. This software generates electrical circuit equations analyzed using simulation program with integrated circuit emphasis (SPICE) from a two-dimensional map, representing a slice of living tissue. Each pixel of the two-dimensional map represents electrode, extracellular medium or intracellular medium, and is modeled with pure resistors. At intracellular–extracellular medium interfaces, a cell membrane is modeled as a capacitance and resistance in parallel. Simulation parameters used were: 30×30 pixels, slice thickness = 50 μ m, pixel size = 5 μ m, membrane capacitance = 1 μ F cm⁻² [27], intracellular medium resistivity = 100 Ω cm [28], extracellular medium resistivity = 100 Ω cm, electrode resistivity = 0.01 Ω cm, frequency range = 100 Hz to 1 MHz.

2.8. Statistical analysis

In order to avoid the assumption that either the impedance modeling parameters or the fluorescent intensity were normally distributed, Spearman's rank-order method was used. For all tests, $p < 0.05$ was considered significant.

3. Results

3.1. Qualitative observations of the tissue response

There was a large variation in the tissue responses to the microwires. These ranged from a tight network of astrocytes only a few cell layers in thickness (figure 3(a)) to reactions extending several hundred μ m from the electrode (figure 3(b)). Similarly, there was a large variation in cellular density as indicated by DAPI staining.

3.2. In vivo impedance spectroscopy

In order to minimize the contribution of electrode polarization to the measurement at low frequencies, the impedance contribution of the electrodes should be small in comparison

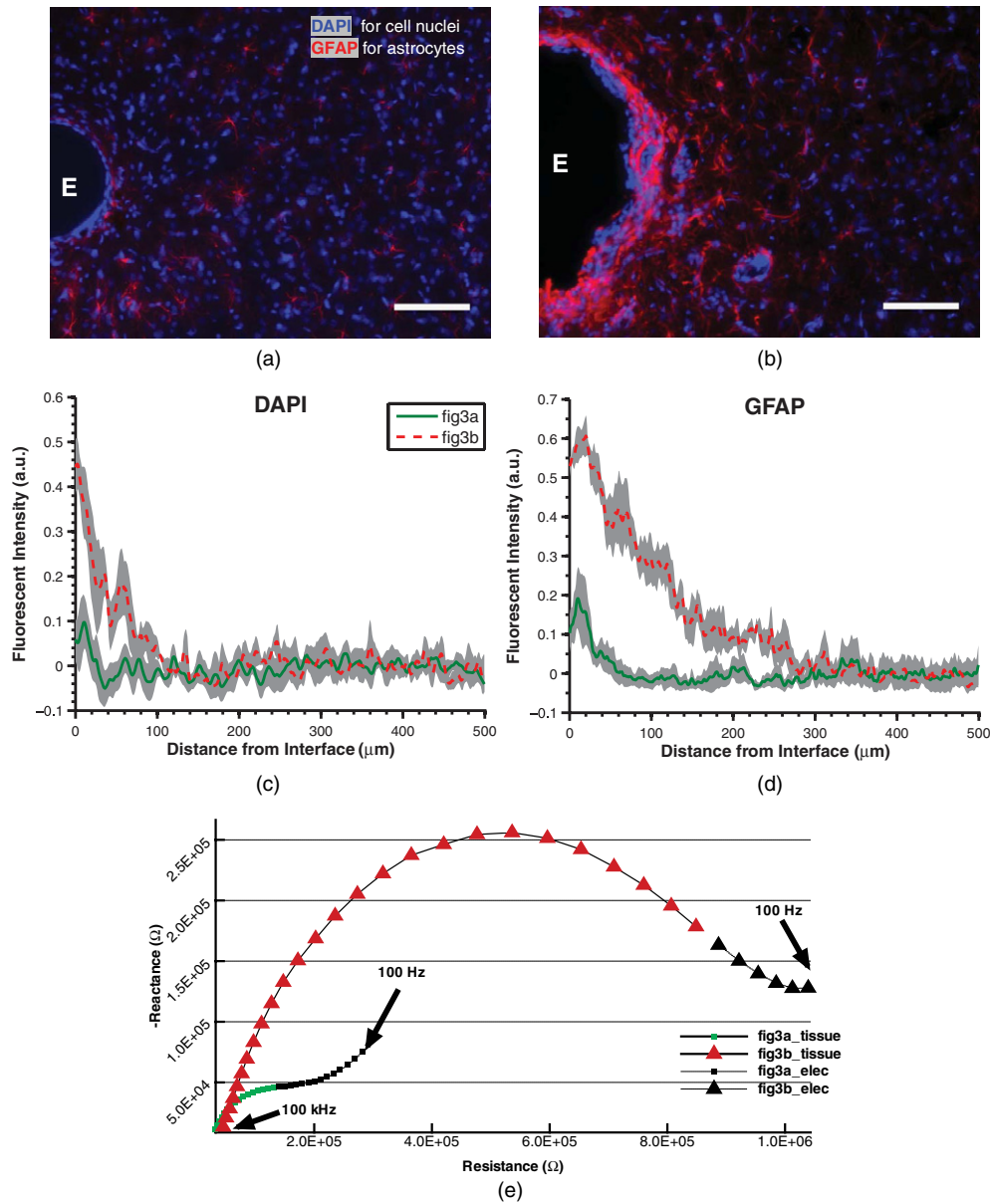


Figure 3. Example immunostained sections showing (a) mild and (b) severe tissue response with fluorescent intensity line profiles for (c) DAPI and (d) GFAP. (e) The corresponding impedance spectra for (a) and (b) show that severe reactions result in broader circular arc loci. (a)–(b) ‘E’s indicate the locations of the electrode tracks. Scale bar = 100 μm. (c)–(d) Mean ± SEM (SEM indicated by gray filled area surrounding lines) of fluorescent pixel intensity as a function of distance from the tissue edge. (e) Green squares correspond to electrode in (a), with $R_o = 251 \text{ k}\Omega$, $R_\infty = 14.5 \text{ k}\Omega$, $f_c = 2819 \text{ Hz}$, $\alpha = 0.61$, $P_y = 0.9422$ and $|Z|_{1 \text{ kHz}} = 182 \text{ k}\Omega$. Red triangles correspond to electrode in (b), with $R_o = 1035 \text{ k}\Omega$, $R_\infty = 28.9 \text{ k}\Omega$, $f_c = 1849 \text{ Hz}$, $\alpha = 0.78$, $P_y = 0.9721$, and $|Z|_{1 \text{ kHz}} = 721 \text{ k}\Omega$. Black filled points were not included in the Cole model, since at these lower frequencies electrode impedance decreased the goodness of fit to the Cole model due to electrode polarization.

to the biological component in a two-electrode measurement system. Impedance measurements in saline after removal of the electrodes from the brain demonstrated that the electrode contribution was orders of magnitude smaller than the tissue at frequencies fitted with the Cole model (data not shown).

Figure 3(e) shows sample impedance spectra from two different electrodes corresponding to the reactions imaged in figures 3(a) and (b). More extensive tissue reactions were associated with a more pronounced circular arc in the loci plots.

3.3. Quantitative correlation of impedance parameters with histology

Table 1 presents the correlations of R_o , R_∞ , f_c , α , P_y and $|Z|_{1 \text{ kHz}}$ with the total intensity of GFAP and DAPI-labeled images for incremental radial distances away from the electrodes. This table shows that the data are significantly correlated only in the immediate vicinity of the electrode (0–100 μm from the interface) for R_o , P_y and $|Z|_{1 \text{ kHz}}$ (see figure 4(a)). Parameters f_c and α are leaning toward

Table 1. Results of Spearman’s ρ correlation between model parameters with GFAP intensity and DAPI intensity as a function of distance away from the tissue edge. Immunostaining of sections with the primary antibody omitted was not significantly correlated with model parameters at any distance, suggesting that the significant correlations between R_o , $|Z|_{inf}$ and P_y with GFAP at 0–100 μm away from the electrode are not due to non-specific binding. Bold text indicates conditions at which the correlation was significant ($p < 0.05$; $n = 8$).

Distance from interface (μm)	Astrocytes (GFAP)		Cell nuclei (DAPI)		2ndary antibody only	
	Spearman’s coefficient (ρ)	p -value	Spearman’s coefficient (ρ)	p -value	Spearman’s coefficient (ρ)	p -value
0–100^{R_o}	0.785 7	0.027 9	0.571 4	0.151	0.047 62	0.935
0–100 ^{R_∞}	0.166 7	0.703	−0.095 24	0.840	0.476 2	0.243
0–100 ^{F_c}	−0.690 5	0.069 4	−0.476 2	0.243	−0.047 62	0.935
0–100 ^α	0.690 5	0.069 4	0.547 6	0.171	0.404 8	0.327
0–100^{P_y}	0.881 0	0.007 24	0.761 9	0.036 8	−0.071 43	0.882 0
0–100^{Z_{1kHz}}	0.738 1	0.045 8	0.547 6	0.171	0.119 0	0.793
300–500 ^{R_o}	0.404 8	0.327	0.309 5	0.462	−0.523 8	0.197
300–500 ^{R_∞}	0.071 43	0.883	−0.261 9	0.536	0.023 81	0.977
300–500 ^{F_c}	−0.309 5	0.462	−0.119 0	0.793	0.476 2	0.243
300–500 ^α	0.214 3	0.619	−0.190 5	0.665	−0.095 24	0.840
300–500 ^{P_y}	0.023 81	0.977	0	1	−0.357 1	0.389
300–500 ^{Z_{1kHz}}	0.261 9	0.536	0.142 9	0.752	−0.404 8	0.327

^{P_y} Correlation with P_y .
^{R_o} Correlation with R_o .
^{R_∞} Correlation with R_∞ .
^{F_c} Correlation with f_c .
^α Correlation with α .
^{Z_{1kHz}} Correlation with $|Z|_{1\text{ kHz}}$.

Table 2. Results of Cole model parameters, P_y , and impedance magnitude at 1 kHz ($|Z|_{1\text{ kHz}}$) for computer simulated data with varying cell density and cell hypertrophy (see figure 5). An increase in cell volume fraction due to increasing either cell density or cell hypertrophy results in an increase in complex impedance, particularly at low frequencies. The parameters most sensitive to changes in cell density and cell hypertrophy are R_o , $|Z|_{1\text{ kHz}}$, f_c and P_y , while R_∞ and α show slighter changes.

		Cole model parameters					
		R_o	R_∞	f_c	α	P_y	$ Z _{1\text{ kHz}}$
Cell density	Low	41 854	18 960	179 750	0.9307	0.547	41 811
	Medium	51 006	19 033	149 690	0.9308	0.627	50 939
	High	59 901	19 144	136 580	0.9389	0.680	59 823
Cell hypertrophy	Low	77 272	19 241	82 098	0.9497	0.751	77 164
	Medium	127 160	19 510	47 394	0.9500	0.847	126 930
	High	229 270	19 813	25 232	0.9466	0.914	228 680

significance in the 0–100 μm range (both $p = 0.0694$), while R_∞ is not significant at any distance.

3.4. Computer modeling

To provide further insight into the mechanisms of cell density and cell hypertrophy on impedance spectra, computer simulations were carried out. Figure 5 shows the constructed modeled tissue slices with corresponding impedance spectra for increasing cell density (a)–(d) and cell hypertrophy (e)–(h). These simulations show that an increase in cell volume fraction, occurring as a result of either increased cell density or cell hypertrophy, produces an increase in the P_y value, R_o , $|Z|_{1\text{ kHz}}$, and characteristic frequency, f_c , of the resulting impedance spectra (see table 2).

4. Discussion

In this study, we present data supporting the use of impedance spectroscopy to non-invasively quantify cellular

concentration in the immediate vicinity of the electrode. Impedance spectroscopy was used to monitor chronically implanted microwire electrodes and three parameters, P_y , R_o and $|Z|_{1\text{ kHz}}$ were found to strongly correlate with GFAP expression, with P_y correlating with cellular density as well. Modeling studies show that cell volume fraction, as influenced by cell density and cell hypertrophy, has a large influence on the impedance spectra, and the P_y , R_o , $|Z|_{1\text{ kHz}}$ and f_c parameters in particular.

It is likely that astrocytes are the largest cellular contributor to the electrode impedance locus, because of the tight interstitial spaces that these cells form within the astroglial scar, which entirely encapsulates the electrode. The astroglial scar restricts the flow of current through the extracellular space, since cell membranes impede current flow at low frequencies. Several studies have investigated the diffusion properties of the extracellular space in the central nervous system (CNS), and in astroglial scar there is an increase in tortuosity [29–31]. Our results corroborate previously reported correlations between

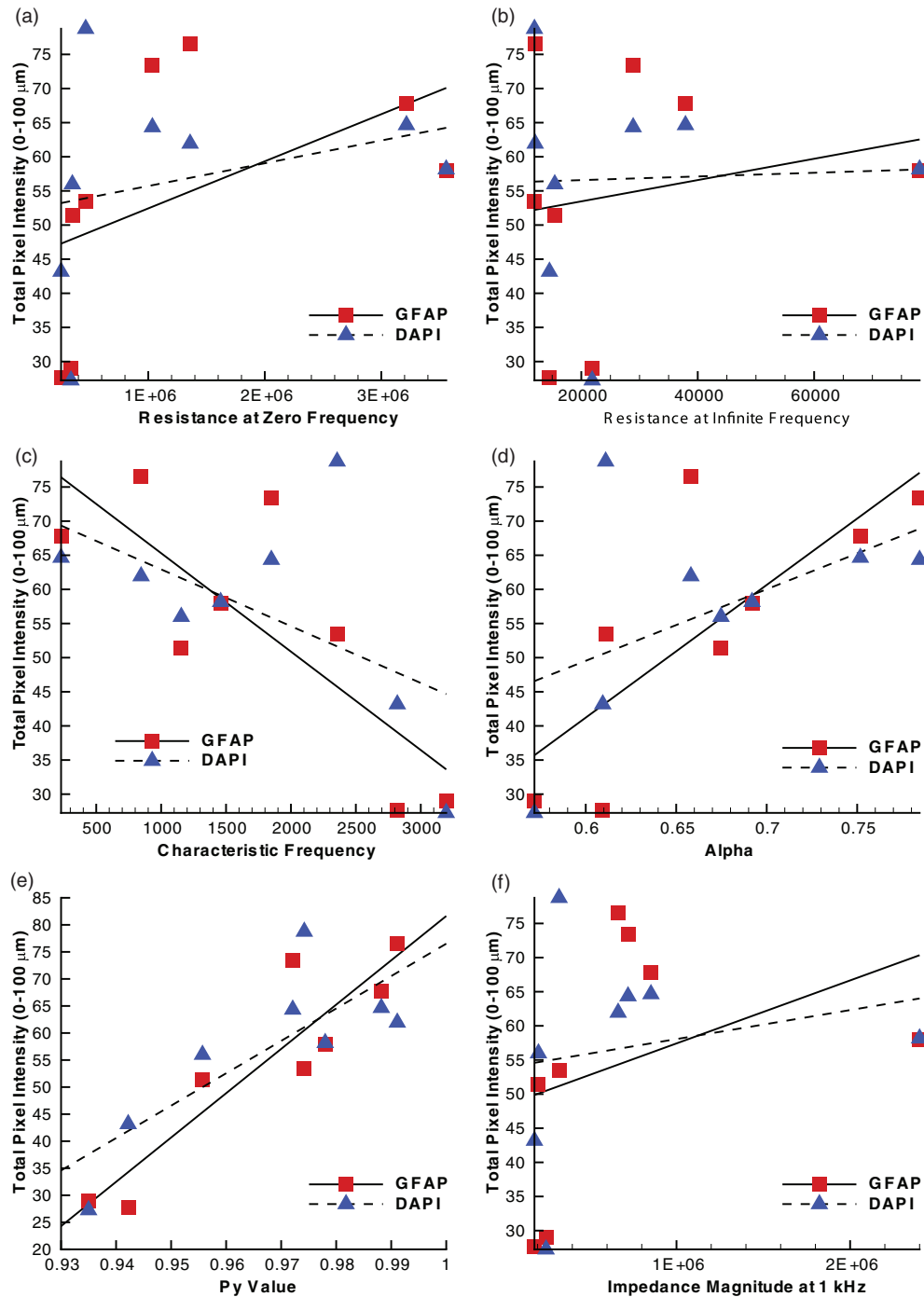


Figure 4. Scatter plot of impedance parameters (a) R_o , (b) R_∞ , (c) f_c , (d) α , (e) Py and (f) $|Z|_{1\text{ kHz}}$ versus GFAP pixel intensity and versus DAPI pixel intensity 0–100 μm from the tissue–electrode interface. Black lines show the linear regression for GFAP (solid) and DAPI (dashed).

impedance spectroscopy and histology [14]. Particularly, our results are consistent with earlier work by Williams *et al* in demonstrating that a more reactive response to microelectrodes results in a more pronounced circular arc in the impedance spectra. In this paper, we additionally characterize the circular arc in the impedance spectra using well-established modeling methods in the bioimpedance literature. This then, along with quantitative histology, allowed us to investigate which

features of the impedance spectra best correlate with the tissue response.

The diameters of the electrode tracts were larger than the electrode diameter in the case of the highest GFAP and DAPI responses. The images from figure 3 were taken at the same magnification and the same size electrodes were used. The electrode track in figure 3(a) is $\sim 175 \mu\text{m}$ in diameter. The discrepancy of 25 μm less than the 200 μm diameter electrode

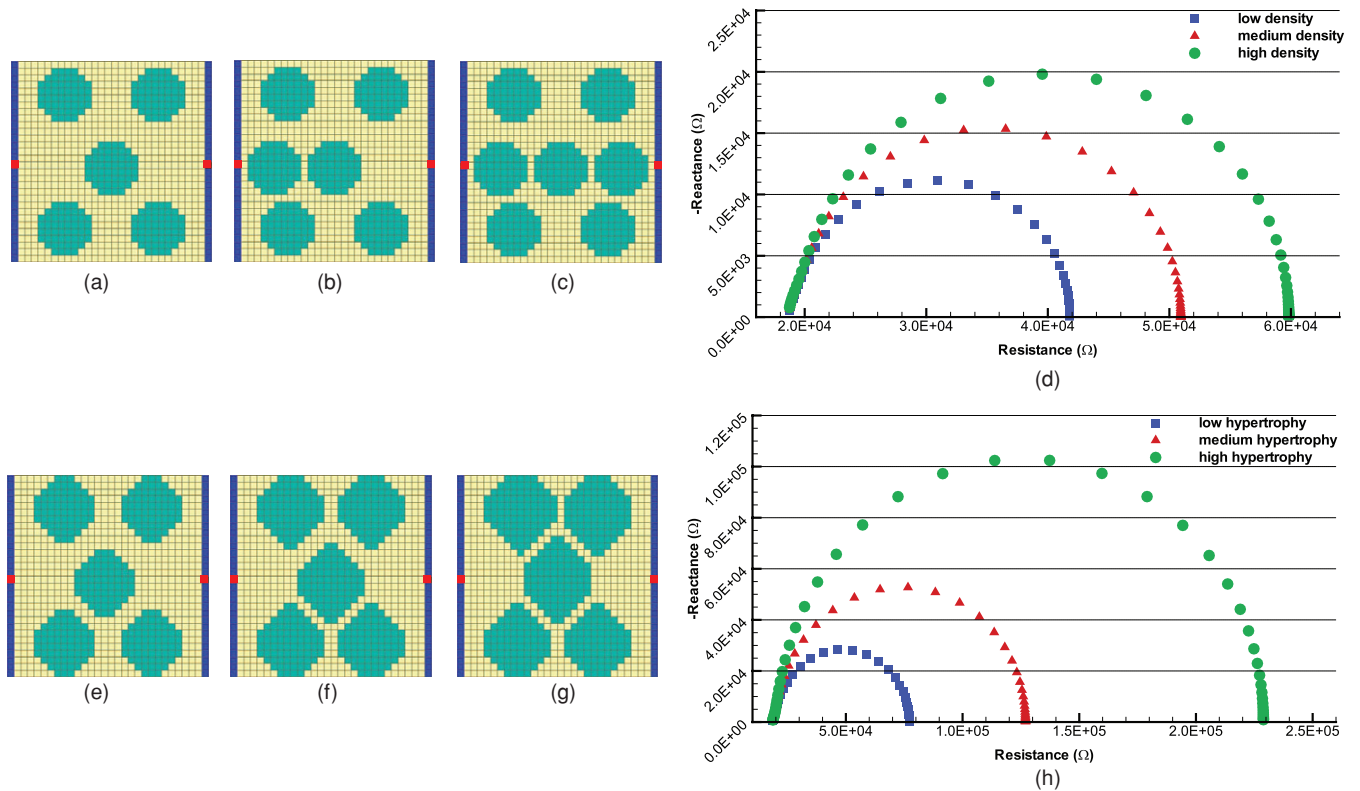


Figure 5. Computer simulations demonstrate the effect of an increase in cell density (low (a) medium (b) and high (c)) and the effect of an increase in cell hypertrophy (low (e), medium (f) and high (g)) on impedance spectra ((d) and (h), respectively). (a)–(f) Green pixels indicate the intracellular medium, yellow pixels indicate the extracellular medium, and blue pixels indicate the electrode. The electrical impedance is calculated between the two red pixels (left: electrode, right: ground). The simulated impedance data were characterized using the same methods used for experimental data (see table 2).

may be due to tissue contraction caused by the fixative. The larger diameter track in figure 3(b) was likely caused by a documented phenomenon in vigorous tissue reactions known as cavitation [32]. Fitch *et al* showed *in vivo* that stimulating microglia activation (using zymosan particles) led to increased levels of reactive astrocytes and cavitation. The size of the cavity, caused by secondary injury due to inflammation, is proportional to the reactive astrocytic response at the edge of the cavity. For this reason, we defined the interface as the edge of the tissue in order to capture the higher-intensity responses of those reactions associated with cavitation.

The 200 μm microelectrode diameter used in our studies is larger than similar recent reports [14, 33]. The larger diameter potentially amplified the intensity and/or variability of the tissue responses after 11 weeks since increased vascular damage, at least during insertion, would be expected. One study reported that sustained tissue responses to devices of differing surface areas are similar (>6 weeks), though the early responses (1–3 weeks) differ [5]. Szarowski *et al* found no difference in tissue response to electrodes with surface areas 2500, 10 000 and 16 900 μm^2 after 6 and 12 weeks post implantation. Differences in tissue response due to the larger surface area of a 200 μm electrode ($\sim 31\,420\ \mu\text{m}^2$) are possible and the influence of electrode dimensions on tissue damage/variability warrants further investigation.

Traditionally, the impedance magnitude measured at 1 kHz has been used as an estimate of chronic recording

electrode performance [23, 34, 35]. Our results predict stronger correlations with the multi-frequency impedance model parameters R_o and P_y . Using a two-electrode impedance measurement configuration, electrode polarization is measured in addition to the surrounding tissue. The effect of electrode polarization on impedance measurements is significant up to 1 kHz [36]. These results, therefore, illustrate an advantage of a multiple frequency modeled approach over a measurement at a single frequency such as 1 kHz, since the model is based on higher-frequency measurements where the effect of electrode polarization is greatly decreased. In a previous study using the Utah electrode array, signal-to-noise ratio (SNR) and $|Z|_{1\text{kHz}}$ were negatively correlated within each monkey, but not across monkeys [37]. One potential explanation for the lack of correlation across animals is impedance differences in the electrodes themselves and not the surrounding tissue. Impedance measurement at multiple frequencies across a wide frequency range is necessary to separate the impedance contribution of the electrode alone from that of the surrounding tissue.

The frequency at which the impedance reactance is maximal, f_c , has been cited as being more stable than either the complex or real impedance values alone [16–18]. Cole parameters have previously been used to characterize ischemia [19]. In this study, R_o and f_c were the two parameters that best characterized ischemia.

A disadvantage of any two-electrode measurement system is that the contribution of the electrode impedance may be larger than the contribution of the tissue impedance at low frequencies (<1 kHz). Future systems using three- or four-electrode designs to minimize or eliminate the contribution of electrode polarization from the measurement may open the possibility for simpler measurements such as $|Z|_{1\text{ kHz}}$ and R_o to be more highly predictive of tissue response. Without the influence of electrode polarization, simulations suggest that these parameters are correlated with cell density and hypertrophy (figure 2). R_∞ changes little, since the resistance at high frequencies is independent of cell membranes, and intra- and extra-cellular resistances are comparable. The disadvantage of the three- and four-electrode measurement setups is the increased complexity of the measurement procedure and calculations.

To investigate whether or not the observed trends in impedance parameters could be produced by cell volume fraction, a computational model was used. The primary limitations of the model are that it does not account for the electrode interface and that it is two dimensional. Since surface area of the cells is proportional to membrane capacitance, it is important to consider how the surface area of the two-dimensional model relates to the *in vivo* three-dimensional cell surface area. The ratio of surface area to volume of a sphere scales with $3/r$. The ratio of circumference to area for a circle, on the other hand, scales with $2/r$. Use of the model to show that the trends are similar is therefore justified, since $2/r$ and $3/r$ scale similarly from this perspective.

The modeled parameters P_y , R_o and $|Z|_{1\text{ kHz}}$ were only correlated with astroglial scar immediately adjacent to the microelectrode (up to 100 μm away), shedding light on the spatial resolution for this application of bioimpedance spectroscopy. This suggests that the bulk of the impedance measured is due to tissue in this region. Earlier reports of the tissue response to microelectrodes identified astroglial scar as spanning 50–100 μm away from the electrode–tissue interface [4, 25, 38–41], consistent with our findings. These experimental data validate earlier finite element modeling studies that predicted the contribution of impedance to be 90% within the first 50 μm away from the electrode surface in a heterogeneous medium such as astroglial scar [42].

The measurement setup, consisting primarily of a lock-in amplifier, is a relatively inexpensive alternative to commercially available impedance measurement systems previously used to measure impedance at multiple frequencies between chronic electrodes and a skull screw [14, 43, 44]. Commercial systems, on the other hand, can be used ‘out of the box’ and the temporal cost of building a custom system should be considered. For future electrode design, the simplified measurement system used in this work is amenable to miniaturization. On-chip lock-in amplifiers, such as that designed by Moe *et al* [45], could be used to integrate a tissue reaction sensor on the implanted electrode.

For human use, this technique has potential for the real-time monitoring of chronic tissue response to microelectrodes. The technique allows the capability to non-invasively follow the same implant at multiple time points, a necessity for human

use. The small currents applied at the electrode are well below thresholds for eliciting neural activity, and allow the tissue to be probed without the risk of damaging the electrode or the tissue.

Acknowledgments

The authors gratefully acknowledge Edgar Brown, Professor Steve P DeWeerth and Ben Haeffele for their technical assistance. Funding support was provided by the NIH, R01 DC 06849 (RVB) and NS 045072 (RVB), and the NSF, CBET-0348338 (RJB). GTEC, an NSF funded ERC located at Georgia Institute of Technology and Emory University (EEC-9731643), is also acknowledged for the use of core facilities.

References

- [1] Hochberg L R, Serruya M D, Friehs G M, Mukand J A, Saleh M, Caplan A H, Branner A, Chen D, Penn R D and Donoghue J P 2006 Neuronal ensemble control of prosthetic devices by a human with tetraplegia *Nature* **442** 164–71
- [2] Schwartz A B 2004 Cortical neural prosthetics *Ann. Rev. Neurosci.* **27** 487–507
- [3] Polikov V S, Tresco P A and Reichert W M 2005 Response of brain tissue to chronically implanted neural electrodes *J. Neurosci. Methods* **148** 1–18
- [4] Turner J N, Shain W, Szarowski D H, Andersen M, Martins S, Isaacson M and Craighead H 1999 Cerebral astrocyte response to micromachined silicon implants *Exp. Neurol.* **156** 33–49
- [5] Szarowski D H, Andersen M D, Retterer S, Spence A J, Isaacson M, Craighead H G, Turner J N and Shain W 2003 Brain responses to micro-machined silicon devices *Brain Res.* **983** 23–35
- [6] Biran R, Martin D C and Tresco P A 2005 Neuronal cell loss accompanies the brain tissue response to chronically implanted silicon microelectrode arrays *Exp. Neurol.* **195** 115–26
- [7] Biran R, Martin D C and Tresco P A 2007 The brain tissue response to implanted silicon microelectrode arrays is increased when the device is tethered to the skull *J. Biomed. Mater. Res. A* **82** 169–78
- [8] Cornish B H, Thomas B J and Ward L C 1993 Improved prediction of extracellular and total body water using impedance loci generated by multiple frequency bioelectrical impedance analysis *Phys. Med. Biol.* **38** 337–46
- [9] De Lorenzo A, Andreoli A, Matthie J and Withers P 1997 Predicting body cell mass with bioimpedance by using theoretical methods: a technological review *J. Appl. Physiol.* **82** 1542–58
- [10] Cole K S 1940 Permeability and impermeability of cell membranes for ions *Cold Spring Harbor. Symp. Quant. Biol.* **8** 110–22
- [11] Cole K S and Cole R H 1941 Dispersion and adsorption in dielectrics *J. Chem. Phys.* **9** 341–52
- [12] Schwan H P 1957 Electrical properties of tissue and cell suspensions *Adv. Biol. Med. Phys.* **5** 147–209
- [13] Grimnes S and Martinsen Ø G 2008 *Bioimpedance and Bioelectricity Basics* (New York: Academic)
- [14] Williams J C, Hippensteel J A, Dilgen J, Shain W and Kipke D R 2007 Complex impedance spectroscopy for monitoring tissue responses to inserted neural implants *J. Neural Eng.* **4** 410–23

- [15] Ludt H and Herrmann H D 1973 *In vitro* measurement of tissue impedance over a wide frequency range *Biophysik* **10** 337–45
- [16] Blad B 1996 Clinical applications of characteristic frequency measurements: preliminary *in vivo* study *Med. Biol. Eng. Comput.* **34** 362–5
- [17] McGree J M, Duffull S B, Eccleston J A and Ward L C 2007 Optimal designs for studying bioimpedance *Physiol. Meas.* **28** 1465–83
- [18] Osterman K S, Paulsen K D and Hoopes P J 1999 Application of linear circuit models to impedance spectra in irradiated muscle *Ann. NY Acad. Sci.* **873** 21–9
- [19] Casas O, Bragos R, Riu P J, Rosell J, Tresanchez M, Warren M, Rodriguez-Sinovas A, Carreno A and Cinca J 1999 *In vivo* and *in situ* ischemic tissue characterization using electrical impedance spectroscopy *Ann. NY Acad. Sci.* **873** 51–8
- [20] Pliquett F and Pliquett U 1999 Stress action on biological tissue and tissue models detected by the py value *Ann. NY Acad. Sci.* **873** 227–38
- [21] Gander W, Golub G H and Strelbel R 1994 Least-squares fitting of circles and ellipses *BIT* **43** 558–78
- [22] Ward L C, Essex T and Cornish B H 2006 Determination of Cole parameters in multiple frequency bioelectrical impedance analysis using only the measurement of impedances *Physiol. Meas.* **27** 839–50
- [23] Ludwig K A, Uram J D, Yang J, Martin D C and Kipke D R 2006 Chronic neural recordings using silicon microelectrode arrays electrochemically deposited with a poly(3,4-ethylenedioxythiophene) (pedot) film *J. Neural Eng.* **3** 59–70
- [24] Fomekong R D, Pliquett U and Pliquett F 1998 Passive electrical properties of rbc suspensions: changes due to distribution of relaxation times in dependence on the cell volume fraction and medium conductivity *Bioelectrochem. Bioenerg.* **47** 81–8
- [25] McConnell G C, Schneider T M, Owens D J and Bellamkonda R V 2007 Extraction force and cortical tissue reaction of silicon microelectrode arrays implanted in the rat brain *IEEE Trans. Biomed. Eng.* **54** 1097–107
- [26] Ivorra A, Gómez R and Aguiló J 2004 A spice netlist generator to simulate living tissue electrical impedance In *Proc. 12th Int. Conf. on Electrical BioImpedance (Gdansk, Poland, June)* pp 317–20
- [27] Koester J 1991 *Principles of Neural Science* 3rd edn (Norwalk, CT: Appleton & Lange)
- [28] Hovey M M, Bak A F and Carpenter D O 1972 Low internal conductivity of aplysia neuron somata *Science* **176** 1329–31
- [29] Roitbak T and Sykova E 1999 Diffusion barriers evoked in the rat cortex by reactive astrogliosis *Glia* **28** 40–8
- [30] Sykova E 2005 Glia and volume transmission during physiological and pathological states *J. Neural. Transm.* **112** 137–47
- [31] Sykova E, Vargova L, Prokopova S and Simonova Z 1999 Glial swelling and astrogliosis produce diffusion barriers in the rat spinal cord *Glia* **25** 56–70
- [32] Fitch M T, Doller C, Combs C K, Landreth G E and Silver J 1999 Cellular and molecular mechanisms of glial scarring and progressive cavitation: *in vivo* and *in vitro* analysis of inflammation-induced secondary injury after cns trauma *J. Neurosci.* **19** 8182–98
- [33] Nicoletis M A L, Dimitrov D, Carmena J M, Crist R, Lehew G, Kralik J D and Wise S P 2003 Chronic, multisite, multi-electrode recordings in macaque monkeys *Proc. Natl Acad. Sci.* **100** 11041–6
- [34] Merrill D R and Tresco P A 2005 Impedance characterization of microarray recording electrodes *in vitro* *IEEE Trans. Biomed. Eng.* **52** 1960–5
- [35] Vetter R J, Williams J C, Hetke J F, Nunamaker E A and Kipke D R 2004 Chronic neural recording using silicon-substrate microelectrode arrays implanted in cerebral cortex *IEEE Trans. Biomed. Eng.* **51** 896–904
- [36] Miklavcic D, Pavselj N and Hart F X 2006 Electric properties of tissues *Wiley Encyclopedia of Biomedical Engineering* (New York: Wiley) pp 3578–89
- [37] Suner S, Fellows M R, Vargas-Irwin C, Nakata G K and Donoghue J P 2005 Reliability of signals from a chronically implanted, silicon-based electrode array in non-human primate primary motor cortex *IEEE Trans. Neural. Syst. Rehabil. Eng.* **13** 524–41
- [38] Collias J C and Manuelidis E E 1957 Histopathological changes produced by implanted electrodes in cat brains; comparison with histopathological changes in human and experimental puncture wounds *J. Neurosurg.* **14** 302–28
- [39] He W, McConnell G C and Bellamkonda R V 2006 Nanoscale laminin coating modulates cortical scarring response around implanted silicon microelectrode arrays *J. Neural Eng.* **3** 316–26
- [40] Schultz R L and Willey T J 1976 The ultrastructure of the sheath around chronically implanted electrodes in brain *J. Neurocytol.* **5** 621–42
- [41] Shain W, Spataro L, Dilgen J, Haverstick K, Retterer S, Isaacson M, Saltzman M and Turner J N 2003 Controlling cellular reactive responses around neural prosthetic devices using peripheral and local intervention strategies *IEEE Trans. Neural. Syst. Rehabil. Eng.* **11** 186–8
- [42] Williams J C 2001 Performance of chronic neural implants *PhD thesis*
- [43] Johnson M D, Otto K J and Kipke D R 2005 Repeated voltage biasing improves unit recordings by reducing resistive tissue impedances *IEEE Trans. Neural. Syst. Rehabil. Eng.* **13** 160–5
- [44] Otto K J, Johnson M D and Kipke D R 2006 Voltage pulses change neural interface properties and improve unit recordings with chronically implanted microelectrodes *IEEE Trans. Biomed. Eng.* **53** 333–40
- [45] Moe A, Marx S, Bhinderwala I and Wilson D 2004 A miniaturized lock-in amplifier design suitable for impedance measurements in cells *IEEE Sensors (Vienna, Austria)*